Structure and stability of hollow vortex equilibria

Stefan G. Llewellyn Smith[1,2] and Darren G. Crowdy[3]†

[1] Institut de Mécanique des Fluides de Toulouse, UMR CNRS/INPT/UPS 5502, Allée Camille Soula, 31400 Toulouse, France

[2] Department of Mechanical and Aerospace Engineering, Jacobs School of Engineering, UCSD, 9500 Gilman Drive, La Jolla, CA 92093-0411, USA

[3] Department of Mathematics, Imperial College, 180 Queen's Gate, London SW7 2AZ, UK

This paper considers the structure and linear stability of two-dimensional hollow vortex equilibria. Equilibrium solutions for a single hollow vortex in linear and nonlinear straining flows are derived in analytical form using free streamline theory. The linear stability properties of this solution class are then determined numerically and a new type of resonance-induced displacement instability is identified. It is found to be a consequence of the fact that one of the shape distortion modes of a circular hollow vortex has the same frequency as one of the modes corresponding to displacement of the vortex centroid. The instability is observed in the case of an isolated hollow vortex situated in straining flow of order three. We also revisit the hollow vortex row solution due to Baker, Saffman & Sheffield (*J. Fluid Mech.*, vol. 74, 1976, p. 1469), and since it is currently lacking in the literature, we present a full linear stability analysis of this solution using Floquet analysis.

1. Introduction

Exact, analytically tractable solutions to the Euler equations describing vortices are few and far between. Understanding the properties of such solutions gives precious insight into the general dynamics of vortical flows. Many known exact solutions correspond to singular, or non-differentiable, flows and several models of vorticity in two dimensions have these properties: point vortices, vortex sheets and vortex patches are the most common models. Saffman (1992) provides an overview of solutions of this kind. He also mentions another class of two-dimensional vortices, hollow vortices, but only in passing. In this paper we study the structure and stability of some basic hollow vortex solutions in two dimensions.

Our definition of a hollow vortex is an incompressible vortex whose interior is at rest in a frame that may itself be in motion with respect to the laboratory frame. This includes vortices moving uniformly through a fluid, and vortices that rotate about a point. No examples of the latter case are presently known. For the former, the pressure in the vortices is constant, and this is usually the physical condition used to specify the

† Email address for correspondence: sgls@ucsd.edu

boundary conditions determining the shape and properties of the vortex. The boundary of a hollow vortex is a vortex sheet because it separates stationary fluid inside the vortex from moving fluid outside it. Hollow vortices are special cases of Sadovskii vortices (Sadovskii 1971; Moore, Saffman & Tanveer 1988) which have both uniform vorticity in their interior as well as a vortex sheet on the boundary. Since the fluid inside is at rest, its properties are not directly relevant to the basic state, but they will affect its stability.

Only a limited number of hollow vortex solutions have been reported in the literature and, since many of these are exact solutions of the incompressible Euler equations, they are of great theoretical importance: in particular they have served as the basis for constructing compressible solutions by means of a Rayleigh–Janzen expansion with the incompressible solution providing the leading-order term. In this way, Ardalan, Meiron & Pullin (1995) have extended the single hollow vortex row (Baker, Saffman & Sheffield 1976, hereafter BSS), while Moore & Pullin (1987) and Leppington (2006) extended the translating hollow vortex pair of Pocklington (1895).

The stability properties of hollow vortices are naturally of interest. One would not expect to see strongly unstable vortices in physical situations, and the utility of such model vortices might then be questionable. The study by BSS and the Appendix of Saffman & Szeto (1981) (hereafter SS) appear to be the only works that consider issues of stability of hollow vortex configurations. On the matter of stability, it is important to distinguish between stagnant-core vortices that contain fluid, possibly of a different density, and hollow vortices that contain vacuum. Baker (1980) discusses the energetics of the single vortex row of BSS in terms of stagnant-core and hollow vortices. A hollow vortex is not expected to be unstable to Kelvin–Helmholtz instability because there is no fluid inside the vortex to support a pressure field. This is not true for stagnant-core vortices.

It is a simple exercise to show that, for linearized perturbations having time dependence $\exp(\lambda t)$ of an isolated circular hollow vortex with strength Γ and radius a, the eigenvalues $\lambda = \lambda_m^{\pm}$ are

$$\lambda_m^{\pm} = \frac{\Gamma}{2\pi a^2} \sigma_m^{\pm}, \tag{1.1}$$

where m denotes a non-zero integer. These modes are neutrally stable and the non-dimensionalized imaginary eigenvalues are

$$\sigma_m^{\pm} = \mathrm{i}(m \pm |m|^{1/2}), \quad m \neq 0. \tag{1.2}$$

This relation is interesting in two respects: first, notice that $m = 1$ is associated with the two frequencies

$$\sigma_1^+ = 2\mathrm{i}, \quad \sigma_1^- = 0, \tag{1.3}$$

while $m = -1$ produces

$$\sigma_{-1}^+ = 0, \quad \sigma_{-1}^- = -2\mathrm{i}. \tag{1.4}$$

Thus, there are two distinct modes having a zero eigenvalue,

$$\sigma_1^- = \sigma_{-1}^+ = 0, \tag{1.5}$$

and these $m = \pm 1$ modes are both associated with displacement of the vortex centroid with no change in the circular shape of the boundary vortex sheet.

More intriguing, however, is the observation that when $m = 4$, the associated eigenfrequencies are

$$\sigma_4^+ = 6\mathrm{i}, \quad \sigma_4^- = 2\mathrm{i}, \tag{1.6}$$

while $m = -4$ is associated with

$$\sigma_{-4}^+ = -2\mathrm{i}, \quad \sigma_{-4}^- = -6\mathrm{i}. \tag{1.7}$$

Hence, on comparison of (1.3) and (1.4) with (1.6) and (1.7) we notice

$$\sigma_1^+ = \sigma_4^- = 2\mathrm{i}, \quad \sigma_{-1}^- = \sigma_{-4}^+ = -2\mathrm{i}. \tag{1.8}$$

There are therefore two distinct modes with eigenvalue $2\mathrm{i}$, and another two modes sharing the eigenvalue $-2\mathrm{i}$. While the modes with $m = \pm 1$ are displacement modes, those with $m = \pm 4$ modes are associated with shape distortions of the vortex boundary. The observation (1.8) therefore suggests the possibility that, when a hollow vortex is forced in an appropriate way, a resonance might be excited between a displacement mode and a shape distortion mode, both having a common eigenfrequency, that may result in an overall displacement instability of the vortex. This forcing might be due to some imposed ambient flow, or the presence of other vortices. In this paper we demonstrate that such instabilities can indeed be generated. We will refer to any such instabilities as 'resonance-induced displacement instabilities'.

This notion of a displacement instability induced by finite-area effects has been observed before. Dritschel (1985) finds a similar phenomenon in his studies of the stability of finite-area generalizations of the polygonal point vortex arrays of Thomson (1883): a rotating polygonal array of 7 vortices, which is neutrally stable when the array is made up of point vortices, becomes unstable to a displacement instability when the point vortices are replaced by vortex patches, even very small ones. This is a finite-area effect because this displacement instability is absent for a point vortex configuration. Dhanak (1992) argues that there are, in fact, two such instabilities. The origin of the displacement instability studied here for hollow vortices is different to that of Dritschel (1985): here it is due to a resonance between a point vortex displacement mode and a shape distortion mode. For a circular Rankine vortex of uniform vorticity, the analogue of (1.2) is (Saffman 1992)

$$\sigma_m = \frac{\mathrm{i}}{2}(|m| - 1)\operatorname{sgn} m, \quad m \neq 0, \tag{1.9}$$

for which only the $m = \pm 1$ displacement modes share a common zero eigenfrequency, so Dritschel's finite-area instability is not caused by the type of resonance we explore here.

The structure of this paper is as follows. In §2, a single hollow vortex is placed in an ambient straining flow of arbitrary order so that the far-field complex potential $w(z)$ has the form

$$w(z) \to \gamma z^n - \frac{\mathrm{i}\Gamma}{2\pi}\log z + \text{analytic function}, \quad n \geqslant 2. \tag{1.10}$$

Equilibrium configurations are found. For $n \geqslant 2$, we are able to produce a class of closed-form solutions to this problem using free streamline theory combined with conformal mapping. Properties of the solution class for $n = 2$, 3 and 4 are described in §2.3. The linear stability of the solutions is examined in §2.4. The choice $n = 3$ is of special interest because, in that case, the nature of the ambient strain flow is such that, for any non-zero imposed strain, it incites a displacement instability between instability

modes of the hollow vortex having the common eigenfrequency in (1.8). In §3 we go on to reappraise the analytical solution for a single hollow vortex row of BSS. While the original authors comment on the linear stability properties, they restricted attention to shape instabilities and disregarded any displacement modes. The paper by SS also considers the single row stability, but focuses on a complementary, but still restricted, class of disturbances. Since a full analysis of the linear stability problem for a single hollow vortex row is currently lacking in the literature, we present such a treatment in §3 by making use of the methods of Floquet theory.

2. Hollow vortex in an ambient strain

2.1. *Formulation*

First, in an attempt to find evidence of a resonance-induced instability associated with modes with eigenfrequencies (1.8), we consider an isolated hollow vortex situated in an ambient flow that might produce the resonance we seek. For maximum generality we analyse a hollow vortex of circulation Γ, centred at the origin, situated in an nth order straining flow (see figure 1). The flow exterior to the vortex is incompressible and irrotational so it is determined by a complex potential $w(z)$ where the associated velocity field (u, v) is given, in complex form, by the relation

$$u - \mathrm{i}v = \frac{\mathrm{d}w}{\mathrm{d}z}. \tag{2.1}$$

As $|z| \to \infty$, $w(z)$ is assumed to have the behaviour

$$w(z) \to \gamma z^n - \frac{\mathrm{i}\Gamma}{2\pi} \log z + \text{analytic function}, \tag{2.2}$$

for some integer $n \geqslant 2$, where γ is a real positive parameter quantifying the imposed rate of strain and the analytic function decays faster than the strain and circulation terms. Together, (2.1) and (2.2) mean that

$$u - \mathrm{i}v \sim n\gamma z^{n-1}, \quad \text{as } |z| \to \infty. \tag{2.3}$$

The interior of the hollow vortex is dynamically inactive and is assumed to be at constant pressure. We seek solutions in which the vortex is in steady equilibrium. The vortex sheet bounding the constant pressure region must be a streamline and, by the steady form of Bernoulli's theorem and the fact that pressure must be continuous across the sheet (we assume there is no singular force distribution, such as surface tension, on the sheet), the vortex sheet must have uniform strength (Saffman 1992).

The special case $n = 2$ corresponds to a single hollow vortex sitting in a linear strain. A study of such a flow situation, attributed to F. M. Hill, is mentioned by BSS and subsequent authors, but the present authors have not been able to find any permanent record of that study. There is no evidence that any previous investigators have studied the case with $n > 2$, so we believe the solutions we find below are new. It is worth mentioning that exact solutions for a finite-area patch of uniform vorticity (a vortex patch) situated in ambient nth-order straining flows of the form (2.2) have been found by Burbea (1981) and generalize the $n = 2$ solutions due to Moore & Saffman (1971). We will now show that exact solutions also exist for hollow vortices.

2.2. *Conformal mapping*

The problem here is a free boundary problem: the shape of the boundary vortex sheet at equilibrium must be determined as part of the solution. It is therefore convenient
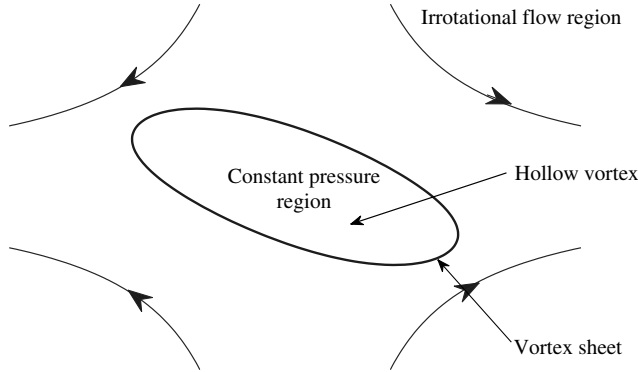
FIGURE 1. Flow schematic: a single hollow vortex in an ambient irrotational strain. The hollow vortex is a finite-area constant pressure region bounded by a vortex sheet.

to introduce a conformal mapping $z(\zeta)$ from the interior of the unit ζ-disc to the unbounded region exterior to the vortex. Without loss of generality, let $\zeta = 0$ map to the point at infinity so that

$$z(\zeta) = \frac{a}{\zeta} + \text{analytic function}, \qquad (2.4)$$

where a is some constant. The circle $|\zeta| = 1$ will map to the vortex sheet making up the boundary of the hollow vortex.

The mathematical problem is to find the complex potential $w(z)$ as well as the functional form of the conformal mapping function $z(\zeta)$. To do this, we employ ideas from free streamline theory. Define the two functions

$$W_0(\zeta) \equiv w(z(\zeta)), \quad R(\zeta) \equiv \frac{\mathrm{d}w}{\mathrm{d}z}. \qquad (2.5)$$

Given $W_0(\zeta)$ and $R(\zeta)$, the conformal mapping is given by the indefinite integral

$$z(\zeta) = \int^{\zeta} \frac{\mathrm{d}W_0(\zeta')}{\mathrm{d}\zeta'} \frac{\mathrm{d}\zeta'}{R(\zeta')}, \qquad (2.6)$$

which follows from the chain rule. In free streamline theory it is traditional to consider the logarithmic function $\log(\mathrm{d}w/\mathrm{d}z)$, often referred to as the Joukowski function (Sedov 1965), but here we consider $R(\zeta) = \mathrm{d}w/\mathrm{d}z$ directly.

The function $W_0(\zeta)$ must be analytic inside $|\zeta| < 1$ except for singularities forced by the far-field condition (2.3). Since the vortex sheet must be a streamline we also require

$$\mathrm{Im}[W_0(\zeta)] = \text{constant on } |\zeta| = 1, \qquad (2.7)$$

where, because the domain is simply connected, the constant can be taken equal to zero without loss of generality. Standard methods, such as the Milne–Thomson circle theorem (Saffman 1992), can be used to deduce that the solution for $W_0(\zeta)$ is

$$W_0(\zeta) = a^n \left(\frac{\gamma}{\zeta^n} + \gamma \zeta^n \right) + \frac{\mathrm{i}\Gamma}{2\pi} \log \zeta. \qquad (2.8)$$

The function $R(\zeta)$ is analytic inside $|\zeta| < 1$ except for a pole of order $n-1$ forced by the far-field condition (2.3). Since the fluid speed must be constant on the vortex

sheet the modulus of $R(\zeta)$ must be constant on $|\zeta| = 1$. It is also expected, from a simple analysis of a point vortex at the stagnation point of the same ambient straining flow, that there will be n stagnation points in the flow (i.e. n zeros of dw/dz). We therefore propose that

$$R(\zeta) = \frac{A}{\zeta^{n-1}} \left(\frac{\zeta^n - \alpha^n}{\zeta^n - \overline{\alpha}^{-n}} \right), \tag{2.9}$$

where $|\alpha| < 1$. It is easy to check that the function $R(\zeta)$ given in (2.9) has constant modulus on $|\zeta| = 1$, a pole of order $n - 1$ at $\zeta = 0$ and n zeros at $\zeta = \alpha \omega_n$, where ω_n denotes the nth roots of unity. Since $dw/dz \to n\gamma z^{n-1}$ as $z \to \infty$, we must pick

$$A = \frac{n\gamma a^{n-1}}{|\alpha|^{2n}}. \tag{2.10}$$

By the chain rule,

$$\frac{dw}{dz} = \frac{dW_0/d\zeta}{dz/d\zeta}. \tag{2.11}$$

Since $dz/d\zeta$ cannot vanish in $|\zeta| < 1$, it follows that any zeros of $R(\zeta)$ in $|\zeta| < 1$ must also be zeros of $dW_0/d\zeta$. Therefore $dW_0/d\zeta$ must have the same zeros as dw/dz. On taking a derivative of (2.8) we find

$$\frac{dW_0}{d\zeta} = \gamma a^n \left(-\frac{n}{\zeta^{n+1}} + n\zeta^{n-1} \right) + \frac{i\Gamma}{2\pi\zeta}, \tag{2.12}$$

and, for this to vanish at $\zeta^n = \alpha^n$, we must have

$$n\gamma a^n \left(-\frac{1}{\alpha^n} + \alpha^n \right) + \frac{i\Gamma}{2\pi} = 0. \tag{2.13}$$

It is easy to check from (2.12) that $dW_0/d\zeta$ also vanishes when $\zeta^n = -\alpha^{-n}$. It follows from the fact, easily seen from (2.12), that $dW_0/d\zeta$ is a rational function of ζ that we can write

$$\frac{dW_0}{d\zeta} = \frac{n\gamma a^n}{\alpha^n \zeta} (\zeta^n - \alpha^n)(\zeta^{-n} + \alpha^n), \tag{2.14}$$

where the prefactor is determined by ensuring that the behaviour as $\zeta \to 0$ of (2.14) is the same as the behaviour of (2.12). Equation (2.11), together with (2.9) and (2.14), then implies that

$$\frac{dz}{d\zeta} = \frac{dW_0/d\zeta}{R(\zeta)} = a(-\zeta^{-2} + (\overline{\alpha}^n - \alpha^n)\zeta^{n-2} + |\alpha|^{2n}\zeta^{2n-2}), \tag{2.15}$$

which can be integrated analytically to give

$$z(\zeta) = a \left[\frac{1}{\zeta} + \frac{\overline{\alpha}^n - \alpha^n}{n-1}\zeta^{n-1} + \frac{|\alpha|^{2n}}{2n-1}\zeta^{2n-1} \right]. \tag{2.16}$$

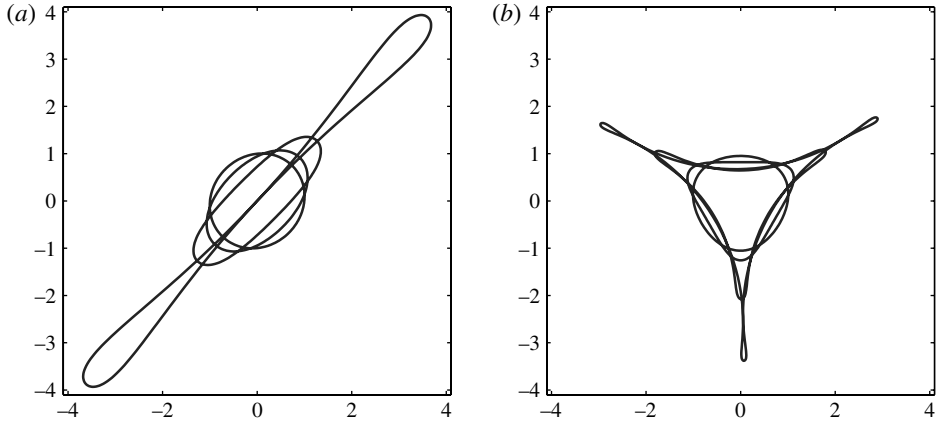An integration constant has been set equal to zero to ensure that the vortex is centred at the origin.

FIGURE 2. Hollow vortex shapes for $n = 2$ with $\mu = 0.05, 0.245, 0.5$ and $\mu = \mu_c^{(2)}$ (*a*) and $n = 3$ with $\mu = 0.1, 0.4, 0.8$ and $\mu = \mu_c^{(3)}$ (*b*). Each vortex has area π.

2.3. *Characterization of the solutions*

Motivated by an analysis of the simpler problem of a point vortex in the same ambient strain, we set

$$\alpha^n = i\beta, \tag{2.17}$$

where β is real and $|\beta| < 1$. Define the non-dimensionalized strain rate parameter

$$\mu = \frac{4n\pi\gamma a^n}{\Gamma}. \tag{2.18}$$

Then (2.13) reduces to

$$\alpha^n + \frac{2i}{\mu} - \frac{1}{\alpha^n} = 0. \tag{2.19}$$

It follows that

$$\beta = -\frac{\mu}{1 + \sqrt{1 - \mu^2}}, \tag{2.20}$$

where $|\mu| < 1$ in order for β be real. The mapping can then be written as

$$z(\zeta) = a\left[\frac{1}{\zeta} - \frac{2i\beta}{n-1}\zeta^{n-1} + \frac{\beta^2}{2n-1}\zeta^{2n-1}\right]. \tag{2.21}$$

For $n = 2$ it is found that hollow vortex equilibria exist for $|\mu| < \mu_c^{(2)} = (3 + 4\sqrt{3})/13 = 0.7637079408$. As shown in figure 2, at $|\mu| = \mu_c^{(2)}$, two distinct parts of the hollow vortex boundary touch each other. For $|\mu| > \mu_c^{(2)}$ the conformal map (2.21) is no longer univalent and the solutions are not physically admissible.

The limiting states for higher values of n have similar properties. For $n = 3$ it is found that hollow vortex equilibria exist for $|\mu| < \mu_c^{(3)} = 0.8939873838$, while for $n = 4$ solutions exist for $|\mu| < \mu_c^{(4)} = 0.9193987084$. In all cases, the limiting solutions arise when different points of the boundary vortex sheet come into contact so that the conformal mapping loses univalence. Typical hollow vortex shapes for $n = 3$, including the limiting shape, are also shown in figure 2. In appendix B, brief details are given as to how the critical parameters $\mu_c^{(n)}$ are determined.
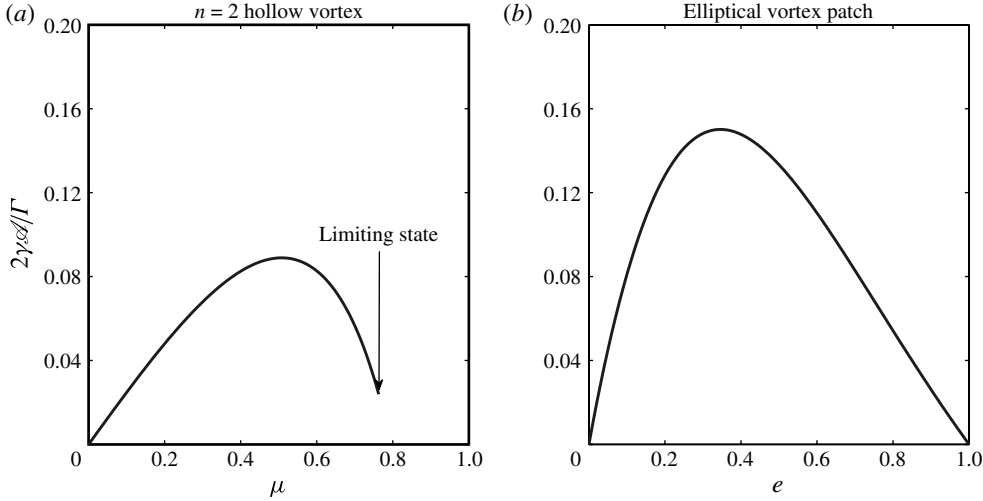
FIGURE 3. (*a*) Graph of $2\gamma\mathscr{A}/\Gamma$ against μ for the $n = 2$ solution: there is a single solution for $0 < 2\gamma\mathscr{A}/\Gamma < 0.0236$, two solutions for $0.0236 < 2\gamma\mathscr{A}/\Gamma < 0.0889$, and no solutions for $2\gamma\mathscr{A}/\Gamma > 0.0889$. (*b*) For comparison, a graph of the same quantity for an elliptical vortex patch as a function of e, the ratio of the lengths of its semi-minor and semi-major axes.

The area $\mathscr{A}$ of each vortex is readily found to be

$$\mathscr{A} = \pi a^2 \left[1 - \frac{4\beta^2}{n-1} - \frac{\beta^4}{2n-1} \right]. \tag{2.22}$$

Figure 3(*a*) shows a graph of the quantity

$$\frac{2\gamma\mathscr{A}}{\Gamma} = \frac{\mu}{4} \left[1 - \frac{4\beta^2}{n-1} - \frac{\beta^4}{2n-1} \right] \tag{2.23}$$

plotted as a function of μ for the case $n = 2$. It shows that there is a single hollow vortex equilibrium for $0 < 2\gamma\mathscr{A}/\Gamma < 0.0236$, there are two equilibria for $0.0236 < 2\gamma\mathscr{A}/\Gamma < 0.0889$ and there are no solutions for $2\gamma\mathscr{A}/\Gamma > 0.0889$. Baker *et al.* (1976) report, based on the work of Hill, that there are two solutions in the interval $0.03 < 2\gamma\mathscr{A}/\Gamma < 0.1$, which is in rough agreement with the results found here.

For purposes of comparison, it is interesting to juxtapose this graph with the analogous one for a vortex patch of uniform vorticity ω_0 in the same straining flow (figure 3*b*). In that case, it is known (Saffman 1992) that the equilibrium vortex patch assumes an elliptical shape with

$$\frac{|2\gamma|}{\omega_0} = \frac{e - e^2}{(1+e)(1+e^2)}, \tag{2.24}$$

where e is the ratio of the semi-minor to semi-major axes of the ellipse. If the patch has area $\mathscr{A}$ then its total circulation Γ is

$$\Gamma = \omega_0 \mathscr{A}, \tag{2.25}$$

so that

$$\frac{|2\gamma|\mathscr{A}}{\Gamma} = \frac{e - e^2}{(1 + e)(1 + e^2)} \tag{2.26}$$

which is the quantity plotted in figure 3(*b*). Relation (2.23) is the analogue, for a hollow vortex, of the known relation (2.26) for an elliptical vortex patch in strain.

If one is interested in the hollow vortex and vortex patch as regularizations of a point vortex of circulation Γ, figure 3 shows that, within both models, admissible regularizations only exist provided the ambient strain rate is not too large, with vortex patches able to sustain a wider range of possible strain rates. The maximum admissible value of $|2\gamma|\mathscr{A}/\Gamma$ is around 0.1501 for vortex patches and 0.0889 for hollow vortices. For a vortex patch, it is always the case that two possible equilibria exist for a given value of $|2\gamma|\mathscr{A}/\Gamma$ in the range $0 < |2\gamma|\mathscr{A}/\Gamma < 0.1501$.

2.4. *Linear stability*

We now study the linear stability properties of the solutions just found. Attention is restricted to irrotational perturbations which introduce no new vorticity into the system; this is predicated on the basis of Kelvin's circulation theorem.

There are two ways to proceed. On the one hand, it is natural to write

$$z(\zeta, t) = z_0(\zeta) + \epsilon\hat{z}(\zeta, t), \quad \mathscr{W}(\zeta, t) = \mathscr{W}_0(\zeta) + \epsilon\hat{\mathscr{W}}(\zeta, t), \tag{2.27}$$

where $\epsilon \ll 1$, $z_0(\zeta)$ and $\mathscr{W}_0(\zeta)$ are, respectively, the conformal map and complex potential for the steady-state equilibria just found, and $\hat{z}(\zeta, t), \hat{\mathscr{W}}(\zeta, t)$ are time-dependent perturbations to them. In this way, the function $z(\zeta, t)$ encodes information on how the equilibrium vortex shape is perturbed and the modified complex potential $\mathscr{W}(\zeta, t)$ gives the associated flow field perturbation. This method is a direct generalization, to unsteady flows, of the method just used to derive the steady solutions and is naturally related to the stability study of streets of finite-cored vortices by Meiron, Saffman & Schatzman (1984). Further details are given in appendix A. Hill (1998) gives other applications of this method. It turns out to be easy to examine the linear stability of the circular case $\gamma = 0$ using this method, and the results are given in § 2.4.1.

A second linear stability method, based on a generalization of the original formulation of BSS, can also be employed and this is described in § 2.4.2 to follow.

All linear stability calculations have been performed independently, using both methods, and the results have been compared for consistency. This lends confidence in the correctness of our results.

2.4.1. *The circular case $\gamma = 0$*

The eigenvalues for the case of a circular hollow vortex with $\gamma = 0$ are readily determined by perturbing the conformal map and complex potential. Let

$$\left.\begin{array}{ll} \hat{z}(\zeta, t) = \hat{a}e^{\lambda t}\zeta^p, & \hat{z}^*(\zeta, t) = \hat{a}^*e^{\lambda t}\zeta^{-p}, \\ \hat{\mathscr{W}}(\zeta, t) = \hat{b}e^{\lambda t}\zeta^{p+1}, & \hat{\mathscr{W}}(\zeta, t)^* = \hat{b}^*e^{\lambda t}\zeta^{-p-1}, \end{array}\right\} \tag{2.28}$$

where $p \geqslant 0$ is an integer, λ is an eigenvalue to be determined and $\hat{a}, \hat{a}^*, \hat{b}$ and $\hat{b}^*$ are independent complex constants. For this case,

$$z_0(\zeta) = \frac{a}{\zeta}, \quad \mathscr{W}_0(\zeta) = -\frac{i\Gamma}{2\pi}\log\zeta. \tag{2.29}$$

Substituting all this into the linearized equations of motion (see appendix A) produces only terms involving ζ^p and ζ^{-p}. On equating coefficients of ζ^p we find

$$\lambda \hat{a} = \mathrm{i}\kappa(p+1)\hat{a} - (p+1)\hat{b}, \quad \lambda \hat{b} = \kappa^2 \hat{a} + \mathrm{i}\kappa(p+1)\hat{b}, \tag{2.30}$$

where $\kappa \equiv \Gamma/(2\pi a^2)$. If $\hat{a}$ is eliminated from both equations it is found that

$$\lambda = \frac{\mathrm{i}\Gamma}{2\pi a^2}(p+1 \pm \sqrt{p+1}), \quad p \geqslant 0. \tag{2.31}$$

Similarly, equating coefficients of ζ^{-p} and performing analogous manipulations gives

$$\lambda = \frac{\mathrm{i}\Gamma}{2\pi a^2}(-p-1 \pm \sqrt{p+1}), \quad p \geqslant 0. \tag{2.32}$$

On letting $m = -p - 1$, we retrieve results (1.1) and (1.2) reported in the Introduction.

2.4.2. *Numerical method*

BSS derive linearized equations to describe the stability of their basic state working in the hodograph plane, i.e. they use the complex variable $W = \phi + \mathrm{i}\psi$ as the independent variable. In this plane, the boundary of the vortex is at $\psi = 0$, so we can denote the perturbation to it as $\psi = \delta(\phi, t)$ and write the perturbation velocity potential as $\Phi(\phi, \psi, t)$. Φ is a harmonic function in $\psi < 0$, decaying as $\psi \to -\infty$. In these coordinates, the dynamic and kinematic boundary conditions are

$$\frac{1}{q_0^2}\frac{\partial \delta}{\partial t} + \frac{\partial \delta}{\partial \phi} = \frac{\partial \Phi}{\partial \psi}, \quad \frac{1}{q_0^2}\frac{\partial \Phi}{\partial t} + \frac{\partial \Phi}{\partial \phi} + \left(\frac{\partial}{\partial \psi}\frac{1}{2}\frac{q^2}{q_0^2}\right)_{\psi=0} \delta = 0. \tag{2.33}$$

The equations (5.4) and (5.5) of BSS are a special form of (2.33). To obtain (2.33), we take the kinematic boundary condition in the W plane and the Bernoulli equation, namely

$$\frac{\mathrm{D}}{\mathrm{D}t}(\psi - \delta) = 0, \quad \frac{p}{\rho} = -\frac{\partial \Phi}{\partial t} - \frac{1}{2}(\nabla\phi + \nabla\Phi)^2, \tag{2.34}$$

where $\mathrm{D}/\mathrm{D}t$ is the material derivative, and linearize them about the basic state on the undisturbed boundary $\psi = 0$, with the disturbance pressure vanishing on the boundary.

Referring back to the complex variable $\zeta = \rho \mathrm{e}^{\mathrm{i}\theta}$, on the streamline $|\zeta| = \rho = 1$, ϕ is a function of θ and the normal derivative of ψ is a function of ρ, so it is convenient to consider the perturbation equations written with θ and ρ as independent variables. Applying the chain rule to (2.33) gives

$$\frac{1}{q_0^2}\frac{\partial \delta}{\partial t} + \frac{1}{\phi_\theta}\frac{\partial \delta}{\partial \theta} = \frac{1}{\psi_\rho}\frac{\partial \Phi}{\partial \rho}, \quad \frac{1}{q_0^2}\frac{\partial \Phi}{\partial t} + \frac{1}{\phi_\theta}\frac{\partial \Phi}{\partial \theta} + \left(\frac{1}{\psi_\rho}\frac{\partial}{\partial \rho}\frac{1}{2}\frac{q^2}{q_0^2}\right)_{\rho=\rho_0} \delta = 0, \tag{2.35}$$

where $\phi_\theta \equiv \partial\phi/\partial\theta$ and $\psi_\rho \equiv \partial\psi/\partial\rho$. From the Cauchy–Riemann equations $\psi_\rho = -\rho^{-1}\phi_\theta$, so we only need the expression

$$\phi_\theta = -\frac{\Gamma}{2\pi}(\mu \sin n\theta + 1), \tag{2.36}$$

which is valid on the vortex boundary and has been derived from the exact solutions. Hence, on letting all coefficients have time dependence $\mathrm{e}^{\lambda t}$, the boundary conditions transform to

$$\sigma \Phi + Q\frac{\partial \Phi}{\partial \theta} = G\delta, \quad \sigma \delta + Q\frac{\partial \delta}{\partial \theta} = -Q\frac{\partial \Phi}{\partial \rho}, \tag{2.37}$$

where $\sigma = 2\pi\lambda a^2/q_0\Gamma$ is the non-dimensional growth rate, and

$$Q = \frac{1}{\phi_\theta} = -\frac{1}{1 + \mu\sin n\theta}, \quad G = Q\left(\frac{\partial}{\partial\rho}\frac{1}{2}\frac{q^2}{q_0^2}\right)_{\rho=\rho_0} = -\frac{1}{1 + \mu\sin n\theta}\text{Re}\,[\zeta S'\overline{S}], \quad (2.38)$$

where S denotes the complex velocity R defined in (2.9) but rescaled to have unit magnitude on the vortex boundary. Indeed, it is straightforward to show from (2.9) that

$$\left.\begin{array}{l} S(\zeta) = \dfrac{1}{\zeta^{n-1}}\dfrac{\zeta^n - \mathrm{i}\beta}{\beta\zeta^n - \mathrm{i}}, \\[3mm] \dfrac{\mathrm{d}S}{\mathrm{d}\zeta} = -\beta\left[\dfrac{(n-1)\zeta^{2n} - \mathrm{i}[(2n-1)\beta - \beta^{-1}]\zeta^n - (n-1)}{\zeta^n(\beta\zeta^n - \mathrm{i})^2}\right]. \end{array}\right\} \quad (2.39)$$

Since Φ is harmonic, the functions Φ and δ can be written in the fluid region as

$$\Phi = \sum_{n=-\infty}^{\infty}\Phi_n\mathrm{e}^{\mathrm{i}n\theta}\rho^{|n|}, \quad \delta = \sum_{n=-\infty}^{\infty}\delta_n\mathrm{e}^{\mathrm{i}n\theta}. \quad (2.40)$$

On substitution of these expressions into the boundary conditions (2.37), we arrive at the matrix equations

$$-\mathrm{i}\sum_{m=-\infty}^{\infty}\hat{Q}_{n-m}m\Phi_m + \sum_{m=-\infty}^{\infty}\hat{G}_{n-m}\delta_m = \sigma\Phi_n, \quad (2.41)$$

$$-\sum_{m=-\infty}^{\infty}\hat{Q}_{n-m}|m|\Phi_m - \mathrm{i}\sum_{m=-\infty}^{\infty}\hat{Q}_{n-m}m\delta_m = \sigma\delta_n. \quad (2.42)$$

These have the truncated form

$$\begin{pmatrix} -\mathrm{i}\boldsymbol{QN} & \boldsymbol{G} \\ -\boldsymbol{Q}|\boldsymbol{N}| & -\mathrm{i}\boldsymbol{QN} \end{pmatrix}\boldsymbol{r} = \sigma\boldsymbol{r} \quad (2.43)$$

in terms of the vector

$$\boldsymbol{r} = [\Phi_{-N}, \ldots, \Phi_0, \ldots, \Phi_N, \delta_{-N}, \ldots, \delta_0, \ldots, \delta_N]^{\mathrm{T}}. \quad (2.44)$$

The function G has been expanded as a Fourier series according to

$$G(\theta) = \sum_{n=-\infty}^{\infty}\hat{G}_n\mathrm{e}^{\mathrm{i}n\theta}, \quad \hat{G}_n = \frac{1}{2\pi}\int_{-\pi}^{\pi}G(\theta)\mathrm{e}^{-\mathrm{i}n\theta}\,\mathrm{d}\theta, \quad (2.45)$$

with Q treated similarly. The matrices $\boldsymbol{N}$, $\boldsymbol{Q}$ and $\boldsymbol{G}$ have the elements

$$\mathcal{N}_{nm} = n\delta_{nm}, \quad \mathcal{Q}_{nm} = \hat{Q}_{n-m}, \quad \mathcal{G}_{nm} = \hat{G}_{n-m}. \quad (2.46)$$

2.4.3. *Results*

Henceforth we will write λ in the non-dimensional form

$$\lambda = \lambda_m^\pm = \frac{\Gamma}{2\pi a^2}\sigma_m^\pm, \quad (2.47)$$

so that, when $\gamma = 0$, the eigenvalues just determined are

$$\sigma_m^\pm = \mathrm{i}(m \pm |m|^{1/2}), \quad m \neq 0, \quad (2.48)$$

where we have substituted $m = p + 1$ so that $m = 1$ now corresponds to the displacement mode, and our notation is now consistent with the discussion in § 1.

The linear stability results for $n = 2$, 3, 4 will now be reported. For $n = 2$, when $\mu > 0$, the configuration for small μ is always unstable to a mode with growth rate $\lambda \approx 2\gamma$. This corresponds to the same displacement mode of instability associated with a point vortex situated at the stagnation point of a linear straining flow. To see this, observe that the complex velocity field associated with a point vortex of circulation Γ at position z_0 in this ambient linear strain is

$$u - \mathrm{i}v = \frac{\mathrm{d}w}{\mathrm{d}z} = 2\gamma z - \frac{\mathrm{i}\Gamma}{2\pi(z - z_0)}, \tag{2.49}$$

so the equation of motion for the point vortex position is

$$\frac{\mathrm{d}\overline{z_0}}{\mathrm{d}t} = 2\gamma z_0. \tag{2.50}$$

This equation is linear in z_0 and, writing $z_0 = \hat{a}\mathrm{e}^{\lambda t}$, it is clear that $\lambda = 2\gamma$. This is the approximate relation for small μ in which the vortex is weakly disturbed by strain. Focussing only on shape instabilities, and disregarding this displacement mode, it is found that the hollow vortices are linearly stable for small μ but a range of μ for which the shape modes become unstable occurs for an interval centred near $\mu = 0.25$. We refer to this as a 'bubble of instability' and, in this bubble, two modes with imaginary part near 9.5 coalesce, producing eigenmodes with non-zero real part. The shape of the vortex at $\mu = 0.245$ is shown in figure 2. The vortices are found to stabilize again as μ increases beyond this bubble, but two more modes coalesce near $\mu = 0.305$ with imaginary parts near 4.512. Beyond this value of μ, the hollow vortices with $n = 2$ are linearly unstable to shape deformations. These results are shown in figure 4. The bubbles of instability where two neutral modes merge is characteristic of Hamiltonian systems (MacKay & Saffman 1986).

For $n = 3$ an analysis of the analogous point vortex problem shows that a point vortex situated at the stagnation point of an $n = 3$ straining flow is linearly neutrally stable. However, the numerical results for the linear stability of a hollow vortex reveals that, for any $\mu > 0$, there is always a quartet of unstable eigenvalues where the real part of σ scales with μ for small μ, while the imaginary parts are close to $\pm 2\mathrm{i}$. Indeed, for small μ it is found numerically that

$$\mathrm{Re}\,\sigma \approx \sqrt{2}\mu. \tag{2.51}$$

Inspection of the eigenvectors corresponding to these unstable eigenvalues reveals that, for small μ, they are indeed a linear superposition of the $m = \pm 1$ and $m = \pm 4$ modes sharing the same eigenfrequencies $\pm 2\mathrm{i}$. This is evidence of the resonance-induced displacement instability associated with the forced interaction of modes having the common eigenfrequencies in (1.8). A perturbation analysis of these unstable modes is given in appendix C. It should be emphasized that this displacement instability is very different to that of the $n = 2$ vortex just discussed because, in that case, the finite-area hollow vortex problem simply inherits the same linear displacement instability exhibited by the analogous point vortex problem. For $n = 3$, the displacement instability is a finite-area effect that vanishes as μ, which scales with the vortex area, tends to zero. If we disregard displacement instabilities, we find that the vortices for $n = 3$ are stable to shape perturbations for $\mu < 0.138$, but these are of dubious physical significance given that the configuration is not structurally stable.
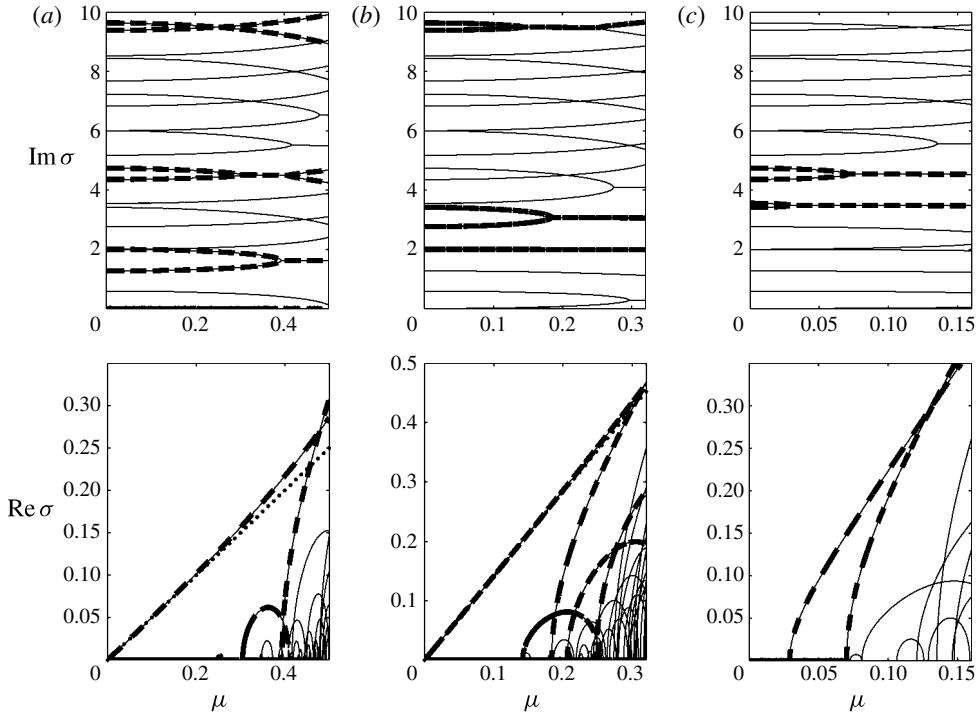
FIGURE 4. Imaginary and real parts of the eigenfrequency σ for the vortex in strain with $n = 2$ (*a*), $n = 3$ (*b*) and $n = 4$ (*c*). Note the difference in the ranges of μ in each case; the picture becomes very complicated for larger μ. The dots correspond to the analytic small-μ limits of the displacement mode $\sigma \approx \mu/2$ for $n = 2$ and $\mathrm{Re}\,\sigma \approx \sqrt{2}\mu$ for $n = 3$. The dashed lines indicate the displacement mode and the first three dominant shape modes. The imaginary parts of σ can be related to the real parts by noticing where two curves coalesce. These results were computed using the method of appendix A with $N = 128$ and were cross-checked against the other method described in § 2.4.2.

In contrast, for $n = 4$ there is no linearly unstable displacement mode for small μ. This is to be expected since a point vortex situated in the stagnation point of such an ambient strain is neutrally stable and, unlike the $m = 4$ eigenmode, the $m = 5$ eigenmode of the single hollow vortex, which would be naturally incited by such an ambient flow, is not resonant with the displacement modes (or, for that matter, any other natural modes). Instead, the vortices become unstable to oscillatory shape deformations at $\mu = 0.0291$ when a quartet of eigenvalues is born with non-zero real part and imaginary parts $\pm 3.482\mathrm{i}$. This instability results from a collision of a pair of purely imaginary eigenvalues at this critical value of μ. This unstable mode does not restabilize before increasingly more modes become unstable for higher values of μ.

In summary, we have presented a detailed linear stability analysis of the equilibria, found earlier in closed form, for an isolated hollow vortex in an nth-order straining flow. The most interesting case is $n = 3$. In that case, distinct modes associated with the natural oscillations of an isolated circular hollow vortex sitting in the absence of strain, and having identical natural frequencies, are forced to resonate when even a small ambient strain rate is switched on. This special resonance incites linear displacement instabilities having growth rates that scale linearly with the ambient strain rate.

3. Single vortex row

Both BSS and SS have treated aspects of the linear stability of the exact solutions of BSS for a single hollow vortex row, but both studies limit the class of perturbations admitted in their analysis. For completeness, we present a complete linear stability analysis of the single hollow vortex row.

First we present a brief review of the exact solutions. By using an approach based on Schwarz–Christoffel mappings in a hodograph plane, BSS constructed a family of exact solutions for a singly periodic row of hollow vortices of spatial period L. BSS find a one-parameter family of solutions parametrized by the dimensionless ratio $R = U_\infty/q_0$ of the velocity at infinity to the fluid speed on the vortex boundary. The shape of any hollow vortex in the singly-periodic row is given parametrically by

$$X = \frac{L}{2\pi}(1 + R^2)\sin^{-1}\left(\frac{2R\sin\lambda}{1 + R^2}\right), \quad Y = \frac{L}{\pi}(1 - R^2)\sinh^{-1}\left(\frac{2R\cos\lambda}{1 - R^2}\right), \quad (3.1)$$

where L is a length scale and $0 \leqslant \lambda < 2\pi$ is a parameter. Small R corresponds to an array of point vortices or a single vortex, while large R gives a vortex sheet. The exterior of the vortex is mapped to the strip $0 < \phi < \Gamma/4$, $\psi < 0$, using symmetry in ϕ. The perimeter length is a non-monotonic function of the distance between the cores and is illustrated in figure 3 of BSS.

3.1. *Approximation by isolated solutions in strain*

Provided the vortices are not too large compared to their separation, it is reasonable to expect that the shapes of typical vortices in this single row will be well approximated by the $n = 2$ solution of §2 with γ, the local strain rate, chosen so that

$$2\gamma = \frac{\pi\Gamma}{6L^2}. \quad (3.2)$$

This is the leading-order approximation to the local strain rate, in the vicinity of any given member of the row, due to the other vortices in the row. This approximation is analogous to the so-called elliptical vortex approximation studied by SS for the case of a single row of vortex patches. The orientation of the $n = 2$ solution (2.21) will not be such that the major axis of the hollow vortex is aligned with the direction of the row, but this is easily fixed by rotating the solution about its centroid. Figure 5 shows typical members of the hollow vortex row found by BSS for $L = \Gamma = 1$ and various choices of hollow vortex area. Superposed on each figure is the solution (2.21), with $n = 2$, having the same area. Condition (3.2), and the area condition, give two equations for parameters μ and a; once these are found, the mapping (2.21) is completely determined. Figure 5 shows that the agreement is good for areas equal to 0.0197 and 0.0758, but it has clearly started to deteriorate when the vortex area is as large as 0.1378. This means that the effects of higher-order strain components are becoming increasingly important. It should be noted that BSS also discuss the idea of approximating the vortices in their row solutions with the solution (attributed to Hill) of isolated vortices in strain.

3.2. *Linear stability analysis*

If the vortices in the row are placed too close together, there is no steady state. BSS conclude that their solutions are unstable for $\beta < 0.434$ (more precisely $\beta_c = 0.433990780\ldots$, the solution to $e^{-\beta}[1 + \log(\coth\beta/2)\sinh\beta] - \cosh\beta = 0$),
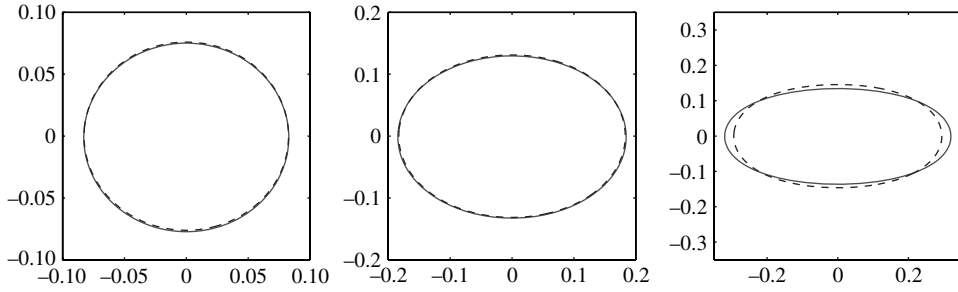
FIGURE 5. Comparison of typical hollow vortices in the single row found by BSS (solid), with $L = \Gamma = 1$, and the $n = 2$ isolated hollow vortex solution (dashed) with condition (3.2) imposed and vortex areas 0.0197, 0.0758 and 0.1378.

where β and R are related by

$$\cosh \beta = \frac{1 + R^4}{2R^2}. \tag{3.3}$$

This condition gives precisely the value that separates the two branches of solutions, and the less deformed shape is stable. BSS explicitly ignored 'disturbances which alter the positions of the vortices'. On the other hand, SS analysed a different restricted class of perturbations, including modes in which alternate vortices move in an identical fashion. They refer to these as 'pairing modes'; when $\beta = \infty$, this is precisely the well-known pairing mode instability of a point vortex row. SS perform an analysis of this instability as β decreases from infinity.

We start from (2.33). In BSS, only 'disturbances with reflexional symmetry about the centre of each vortex' are considered. This corresponds to solutions with period $\Gamma/4\pi$ rather than $\Gamma/2\pi$. Alternatively, BSS consider only even modes. Odd modes are considered in SS. We consider both as part of the Floquet analysis.

Our goal is to solve (2.33) without using the special properties of the basic state that lead to the recurrence relations of BSS and SS. We non-dimensionalize using $\xi = (2\pi/\Gamma)\phi$, $\eta = (2\pi/\Gamma)\psi$ and $\sigma = \lambda\Gamma/(2\pi q_0^2)$, which is different from BSS. The boundary conditions become

$$\sigma \Phi + \frac{\partial \Phi}{\partial \xi} = G(\xi)\delta, \quad \sigma\delta + \frac{\partial \delta}{\partial \xi} = \frac{\partial \Phi}{\partial \eta} \tag{3.4}$$

on $\eta = 0$ and Φ decays as $\eta \to -\infty$. The basic state determines the function

$$G(\xi) = -\frac{(b^2 - 1)^{1/2}}{b - \cos 2\xi}. \tag{3.5}$$

The Floquet analysis follows Deconinck & Kutz (2006). The solution for Φ and δ can be written as

$$\Phi = \sum_{n=-\infty}^{\infty} \Phi_n e^{i(s+n/P)\xi + |s+n/P|\eta}, \quad \delta = \sum_{n=-\infty}^{\infty} \delta_n e^{i(s+n/P)\xi}. \tag{3.6}$$

The integer P is a dummy parameter, in the sense that the stability results are independent of P, provided s is allowed to span the range $(-\pi/P, \pi/P)$. As a result,

on the boundary $\eta = 0$,

$$\Phi_\xi = \sum_{n=-\infty}^{\infty} \mathrm{i}(s + n/P)\Phi_n \mathrm{e}^{\mathrm{i}(s+n/P)\xi}, \quad \Phi_\eta = \sum_{n=-\infty}^{\infty} |s + n/P|\Phi_n \mathrm{e}^{\mathrm{i}(s+n/P)\xi}. \tag{3.7}$$

With $\nu_n = \sigma + n/P$, the two boundary conditions can be rewritten as the matrix equations

$$-\mathrm{i}\nu_n\Phi_n + \sum_{m=-\infty}^{\infty} \hat{G}_{(n-m)/P}\delta_m = \sigma\Phi_n, \tag{3.8}$$

$$|\nu_n|\Phi_n - \mathrm{i}\nu_n\delta_n = \sigma\delta_n. \tag{3.9}$$

If $n - m$ is not divisible by P, the term $G_{(n-m)/P}$ is 0. The resulting truncated finite eigenvalue problem is

$$\begin{pmatrix} -\mathrm{i}\boldsymbol{N} & \boldsymbol{G} \\ |\boldsymbol{N}| & -\mathrm{i}\boldsymbol{N} \end{pmatrix} \boldsymbol{r} = \sigma\boldsymbol{r}. \tag{3.10}$$

The matrix $\mathscr{G}$ has a diagonal structure with non-zero entries along the main diagonal and $P - 1$ zero diagonals between non-zero diagonals. There are always two zero eigenvalues corresponding to constant velocity potential; these are physically irrelevant. Other formulations for the problem are possible; in particular the recurrence relation of BSS comes from dividing one of the equations above by G.

Figure 6(*a,b*) shows the real and imaginary parts of σ for the vortex row for the purely periodic case, i.e. with $s = 0$ and $P = 1$. The instability discussed by BSS corresponds to the solid curve for the real part appearing at $\beta = 0.434$ as the frequency of that mode vanishes. A bubble of instability is visible just to the left of this point. The result of SS corresponds to the (only) dashed curve that exists for large β. This is a resonant instability between the $+1$ and -1 modes with zero imaginary part, as discussed in the Introduction. It is no longer the most unstable mode for $\beta < 0.2743$.

The large-b unstable mode with frequency behaving like b^{-1} is very clear, even though β only goes up to 1. The result $\sigma \sim (4b)^{-1}$ is derived in appendix C. In dimensional terms the growth rate is $\pi\Gamma/4L^2$, recovering that of the pairing instability of a line array of point vortices. We see, however, that the desingularized pairing instability found here manifests itself as a resonance between modes 1 and -1. These modes correspond to displacements of the centres of the vortices. For the full Floquet calculation, one allows s to take all possible values in its range. The results are exactly the same as before. The most unstable mode always corresponds to $s = 0$, and hence to periodic solutions. This may seem different from the pairing instability observed in the vortex patch single row discussed in Kamm (1987) and Saffman (1992) and the statement of SS that the resonant instability of the row corresponds to the pairing instability. However, the Floquet multiplier in the independent variables (ϕ, ψ) is not the physical-space Floquet multiplier. The map from (ϕ, ψ) to (x, y) is two-to-one and its symmetry properties are such that the odd modes, including the unstable mode, are antisymmetric in the physical plane and look like the pairing mode of the vortex row.

To summarize our results, it has been verified, by means of a full Floquet analysis with no approximations on the type of instability, that all prior partial results on the stability of the single hollow vortex row deduced by SS and BSS using special arguments, are indeed correct.
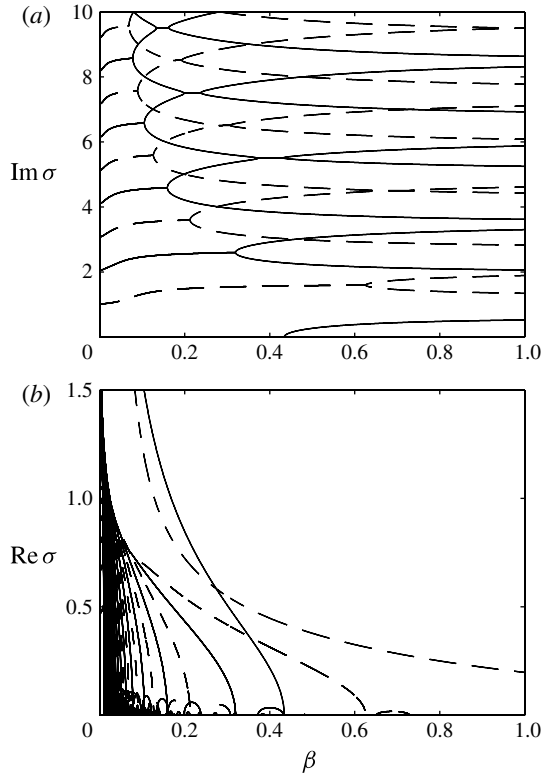
FIGURE 6. Stability of the vortex row of BSS. (*a*) The imaginary part of λ, (*b*) the real part. One half of the modes computed with $N = 128$ with smallest imaginary part in absolute value are plotted. The method of BSS produces only the even modes (solid curves), with the first instability arising around $\beta = 0.43$. The calculation of SS produces only the odd modes (dashed curves), including the resonant mode. Note that Table 4 in Appendix B of SS is limited to the displacement mode alone.

4. Discussion

This paper has studied the structure and stability of hollow vortex equilibria. In particular, we have explicitly demonstrated the existence of a special kind of displacement instability having its origin in the degeneracy of certain eigenfrequencies of a circular hollow vortex. The resonant interaction of a displacement mode with a shape deformation mode can lead to a net displacement instability that is a purely finite area effect and cannot be found in an analogous point vortex problem. This novel instability appears to be peculiar to the hollow vortex model and the authors are not aware of any analogous instabilities in other vortex dynamics systems. Our results offer a cautionary note: if a given point vortex equilibrium is regularized to a 'nearby' equilibrium by replacing all point vortices by small hollow vortices, it is not necessarily the case that this neighbouring equilibrium will share the same structural stability properties as the original point vortex system. The very act of employing the hollow vortex regularization has the potential, as we have shown, to incite new displacement instabilities.

In the last few decades the hollow vortex model has arguably been overtaken by the vortex patch model as the most popular choice for desingularizing a point vortex

in two dimensions. This is perhaps surprising given that, as we have shown here, free streamline theory and conformal mapping can be combined to identify exact solutions for many hollow vortex equilibria. This study is the first report on a wider investigation by the authors on the properties of hollow vortex equilibria. Several other configurations of theoretical interest include the travelling hollow vortex pair in a channel (a generalization of the hollow vortex pair of Pocklington 1895); polygonal hollow vortex arrays, including those with a central hollow vortex and polygonal arrays of satellite vortices; a hollow vortex street; and others. Crowdy & Green (2011) have recently found analytical solutions for a von Kármán vortex street that generalize the single row solution of BSS. The vortex street is particularly interesting given its importance in applications, and the large amount of existing work on the von Kármán vortex street and its generalization to streets of vortex patches (e.g. Saffman & Schatzman 1981; Kamm 1987).

While the equilibrium shapes of hollow vortices apply also to stagnant-core vortices, the stability properties in the two cases are different: for stagnant-core vortices, the dynamical boundary condition has to be modified because the pressure is no longer constant on the boundary when the enclosed fluid is perturbed. Also, a new parameter – the ratio of fluid densities inside and outside the vortex – appears in the formulation. The developments presented in § 3 can be extended to cover this case. Furthermore, stagnant vortices will be unstable to the Kelvin–Helmholtz instability. To regularize this, the natural remedy is to add the effects of surface tension, which will stabilize the interface for the high modes, which are the most unstable ones. However, the basic states we have examined do not include surface tension, and new basic equilibrium states need to be found. These would be generalizations of the isolated hollow vortex solutions with surface tension first derived by Crowdy (1999) and subsequently developed by Wegmann & Crowdy (2000).

The generalization of these vortices to incorporate regions of constant vorticity bounded by vortex sheets is also of interest. Such structures are closely related to Sadovskii vortices. The method of Saffman & Tanveer (1984), or Moore *et al.* (1988), could be adapted to solve the resulting free-boundary problem. An obvious question then is whether these vortices exist for all values of interior vorticity and fluid speed on the boundary. Recent work on hollow vortex wakes behind bluff bodies by Telib & Zannetti (2011) has contributed in this direction and shows the potential of the general ideas.

Finally, given that large classes of hollow vortex equilibria appear to be available in analytical form, it may be convenient to apply recent ideas based on variational arguments, presented by Luzzatto-Fegiz & Williamson (2010), concerning the stability properties of vortex equilibria.

Appendix A. Alternative stability analysis of vortex in strain

This appendix outlines a method for studying the linear stability of the isolated hollow vortex equilibria by perturbing the conformal map and complex potential. We

assume that the equilibrium state undergoes small irrotational perturbations with the same conditions maintained in the far field. It is useful to write the perturbed complex potential as

$$w(z, t) = \gamma z^n - \frac{\mathrm{i}\Gamma}{2\pi} \log z + W(z, t), \tag{A 1}$$

where $W(z, t)$ is analytic as $z \to \infty$. In this way the far-field boundary condition will always be enforced and, because the strain rate γ and circulation Γ are fixed in time,

$$\left.\frac{\partial w}{\partial t}\right|_z = \left.\frac{\partial W}{\partial t}\right|_z, \quad \left.\frac{\partial w}{\partial z}\right|_t = n\gamma z^{n-1} - \frac{\mathrm{i}\Gamma}{2\pi z} + \left.\frac{\partial W}{\partial z}\right|_t. \tag{A 2}$$

Defining $\mathscr{W}(\zeta, t) \equiv W(z(\zeta, t), t)$, we obtain

$$\left.\frac{\partial W}{\partial t}\right|_z = \left.\frac{\partial \mathscr{W}}{\partial t}\right|_\zeta - \frac{\partial z/\partial t|_\zeta}{\partial z/\partial \zeta|_t} \left.\frac{\partial \mathscr{W}}{\partial \zeta}\right|_t. \tag{A 3}$$

The kinematic condition on the hollow vortex boundary is

$$V_n = \boldsymbol{u} \cdot \boldsymbol{n}, \tag{A 4}$$

where V_n is the velocity normal to the boundary. Since, on $|\zeta| = 1$, we can write $\mathrm{d}z/\mathrm{d}s = -\mathrm{i}\zeta z_\zeta |z_\zeta|^{-1}$, where z_ζ denotes the partial derivative with respect to the first argument, (A 4) becomes

$$\mathrm{Re}\left[\frac{\partial z/\partial t}{\zeta z_\zeta}\right] = \mathrm{Re}\left[\frac{\zeta z_\zeta}{|z_\zeta|^2}\left(n\gamma z^{n-1} - \frac{\mathrm{i}\Gamma}{2\pi z} + \frac{\partial \mathscr{W}/\partial \zeta}{\partial z/\partial \zeta}\right)\right]. \tag{A 5}$$

The unsteady Bernoulli condition, in complex notation, takes the form

$$\mathrm{Re}\left[\left.\frac{\partial W}{\partial t}\right|_z\right] = H - \frac{1}{2}\left|\frac{\partial w}{\partial z}\right|^2. \tag{A 6}$$

Using (A 2) and (A 3),

$$\mathrm{Re}\left[\frac{\partial \mathscr{W}}{\partial t} - \frac{\partial z/\partial t}{\partial z/\partial \zeta}\frac{\partial \mathscr{W}}{\partial \zeta}\right] = H - \frac{1}{2}\left|n\gamma z^{n-1} - \frac{\mathrm{i}\Gamma}{2\pi z} + \frac{\partial \mathscr{W}/\partial \zeta}{\partial z/\partial \zeta}\right|^2. \tag{A 7}$$

We now write

$$z(\zeta, t) = z_0(\zeta) + \epsilon \hat{z}(\zeta, t), \quad \mathscr{W}(\zeta, t) = \mathscr{W}_0(\zeta) + \epsilon \hat{\mathscr{W}}(\zeta, t), \tag{A 8}$$

where

$$z_0(\zeta) = r\left(\frac{1}{\zeta} - \frac{2\mathrm{i}\beta}{n-1}\zeta^{n-1} + \frac{\beta^2}{2n-1}\zeta^{2n-1}\right) \tag{A 9}$$

and

$$\mathscr{W}_0(\zeta) \equiv \left[r^n\left(\frac{\gamma}{\zeta^n} + \gamma\zeta^n\right) + \frac{\mathrm{i}\Gamma}{2\pi}\log\zeta\right] - \left[\gamma z_0(\zeta)^n - \frac{\mathrm{i}\Gamma}{\pi}\log z_0(\zeta)\right]. \tag{A 10}$$

We also let $H_0 + \epsilon\hat{H}$, but changes in the Bernoulli constant only result in constants being added to the velocity potential and therefore do not affect the flow in any way. Equations (A 5) and (A 7) are then linearized at $O(\epsilon)$. For brevity, these linearized equations, which are not particularly instructive, will not be written explicitly here.

Following the approach used by Meiron *et al.* (1984) in their linear stability study of streets of finite-cored vortices, we now introduce the decompositions

$$\hat{z}(\zeta, t) = e^{\lambda t}\hat{z}(\zeta), \quad \overline{\hat{z}(\zeta, t)} = e^{\lambda t}\hat{z}(\zeta)^*, \tag{A 11}$$

where we treat $\hat{z}(\zeta)$ and $\hat{z}(\zeta)^*$ as independent functions, and similarly

$$\hat{\mathscr{W}}(\zeta, t) = e^{\lambda t}\hat{\mathscr{W}}(\zeta), \quad \overline{\hat{\mathscr{W}}(\zeta, t)} = e^{\lambda t}\hat{\mathscr{W}}(\zeta)^*, \tag{A 12}$$

where $\hat{\mathscr{W}}(\zeta)$ and $\hat{\mathscr{W}}(\zeta)^*$ are also taken to be independent.

For values of ζ on the unit circle we also write

$$\hat{z}(\zeta) = \frac{\hat{a}}{\zeta} + \sum_{k=0}^{N/2-2} \hat{a}_k\zeta^k, \quad \hat{z}(\zeta)^* = \frac{\hat{a}^*}{\zeta} + \sum_{k=0}^{N/2-2} \hat{a}_k^*\zeta^{-k}, \tag{A 13}$$

where N is a truncation parameter and the $N/2$ coefficients $\{\hat{a}, \hat{a}_k \mid k = 0, 1, \ldots, N/2 - 2\}$ and the $N/2$ coefficients $\{\hat{a}^*, \hat{a}_k^* \mid k = 0, 1, \ldots, N/2 - 2\}$ are to be determined. Also, let

$$\hat{\mathscr{W}}(\zeta) = \sum_{k=1}^{N/2-1} \hat{b}_k\zeta^k, \quad \hat{\mathscr{W}}(\zeta)^* = \sum_{k=1}^{N/2-1} \hat{b}_k^*\zeta^{-k}, \tag{A 14}$$

where the $N/2 - 1$ coefficients $\{\hat{b}_k \mid k = 1, \ldots, N/2 - 1\}$ and the $N/2 - 1$ coefficients $\{\hat{b}_k^* \mid k = 1, \ldots, N/2 - 1\}$ are to be determined. Notice that we have truncated the expansions of the perturbation to the mapping, and that of the complex potential, at different orders; this is motivated by the analytical result for a circular hollow vortex presented in § 2.4.1. Also, we have ignored the constant term in the potential because this just determines $\hat{H}$, and this is not physically significant. The total number of complex unknowns is $2(N/2 + (N/2 - 1)) = 2N - 2$.

To fix a rotational degree of freedom in the Riemann mapping theorem we set

$$\hat{a}^* = \hat{a}. \tag{A 15}$$

This represents one equation. Equating coefficients of ζ^j for $-(N/2) + 1 \leqslant j \leqslant N/2 - 1$ in the kinematic condition gives $N - 1$ additional equations. Finally, equating coefficients of ζ^j for $-(N/2) + 1 \leqslant j \leqslant N/2 - 1$ in the Bernoulli condition, but ignoring the constant term, gives $N - 2$ equations. In total we then have $1 + (N - 1) + (N - 2) = 2N - 2$ equations for the $2N - 2$ unknowns.

The linear stability spectrum is found by rewriting the linearized equations, having substituted the forms (A 13) and (A 14), in the matrix form

$$\boldsymbol{A}\boldsymbol{x} = \lambda\boldsymbol{B}\boldsymbol{x}, \tag{A 16}$$

where $\boldsymbol{x}$ is a vector in which the $2N - 2$ unknown coefficients are collected. $\boldsymbol{A}$ and $\boldsymbol{B}$ are matrices dependent on the base state equilibrium solution, whose entries can be conveniently determined with the aid of fast Fourier transforms.

Appendix B. Determination of critical parameters $\mu_c^{(n)}$

To compute the critical value of μ at which the mapping (2.21) is no longer univalent, we take advantage of the fact that (2.21) is a rational mapping. For each

point $\zeta_c = e^{i\phi}$ on the boundary of the unit circle, we solve the polynomial equation

$$p(\zeta) = \zeta \left(\frac{z(\zeta) - z(\zeta_c)}{\zeta - \zeta_c} \right) = \frac{\beta^2}{2n-1} (\zeta^{2n-1} + \zeta_c \zeta^{2n-2} + \cdots + \zeta_c^{2n-2} \zeta)$$

$$- \frac{2i\beta}{n-1} (\zeta^{n-1} + \zeta_c \zeta^{n-2} + \cdots + \zeta_c^{n-2} \zeta) - \frac{1}{\zeta_c} = 0. \quad \text{(B 1)}$$

By construction, this polynomial has roots outside the unit disc when the mapping is univalent, and certainly for small μ. For each value of ϕ, we find the value of β for which the roots of (B 1) with smallest modulus has modulus 1. We then minimize β over all ϕ. The result is the value of β, and hence μ, at which a point of the mapping has two pre-images on the unit circle, i.e. the value at which the mapping is no longer univalent. This technique is guaranteed to work for rational mappings. For transcendental mappings, the equation corresponding to (B 1) is no longer a polynomial, and hence might have an infinity of roots. Provided one can identify the smallest root in magnitude, the method will still work.

Appendix C. Resonant instability of near-circular vortices

The small-μ limit of the vortex in strain and the large-b limit of BSS both correspond to near-circular vortices. From figure 4 it is clear that the growth rate for $n = 2$ and $n = 3$ is proportional to μ for small μ, and that vortices with larger n are stable for small μ, as predicted in §1. An informal argument showed that for $n = 2$, the result was $\sigma \sim (1/2)\mu$. SS shows, using their recurrence relation, that in the large-b limit the growth rate for BSS goes as $(4b)^{-1}$. We sketch the approach for BSS using the governing equations and then give a general formulation in matrix form.

Expanding $G(\xi)$ in b gives

$$G(\xi) = -1 - b^{-1} \cos 2\xi + O(b^{-2}). \quad \text{(C 1)}$$

At $O(b^{-1})$ the governing equations become

$$\sigma_0 \Phi_1 + \sigma_1 \Phi_0 + \frac{\partial \Phi_1}{\partial \xi} = -\delta_1 - \cos 2\xi \delta_0, \quad \sigma_0 \delta_1 + \sigma_1 \delta_0 + \frac{\partial \delta_1}{\partial \xi} = \frac{\partial \phi_1}{\partial \eta}. \quad \text{(C 2)}$$

The basic-state flow leads to the $\cos 2\xi \delta_0$ term, which will couple modes. To obtain the growth rate, we consider the two modes with $\sigma = 0$ and write

$$\Phi_0 = a_+ e^{i\xi + \eta} + a_- e^{-i\xi + \eta}, \quad \delta_0 = -i a_+ e^{i\xi} + i a_- e^{-i\xi}. \quad \text{(C 3)}$$

The $O(b^{-1})$ solutions take the form

$$\Phi_1 = b_+ e^{i\xi} + b_- e^{-i\xi} + \cdots, \quad \delta_1 = c_+ e^{i\xi} + c_- e^{-i\xi} + \cdots, \quad \text{(C 4)}$$

where other harmonics have not been given explicitly. Substituting (C 4) into (C 2) and enforcing a solvability condition leads to four homogeneous equations in the four unknowns b_+, b_-, c_+ and c_-. The resulting determinant condition is $\sigma_1^2 = 1/2$, which has real roots, so we have instability.

Formally, we can expand the matrix equation (3.10) and obtain

$$\left[\begin{pmatrix} -i\mathbf{N} & -\mathbf{I} \\ |\mathbf{N}| & -i\mathbf{N} \end{pmatrix} + b^{-1} \begin{pmatrix} 0 & \mathbf{C}_2 \\ 0 & 0 \end{pmatrix} + \cdots \right] \mathbf{r} = (\mathbf{A} + b^{-1}\mathbf{B} + \cdots)\mathbf{r} = \sigma \mathbf{r}, \quad \text{(C 5)}$$

where $\mathbf{C}_2$ is the matrix corresponding to the Fourier transform of $\cos 2\xi$, namely $[\mathbf{C}_2]_{nm} = (1/2)(\delta_{n,m+2} + \delta_{n,m-2})$. This is a perturbation eigenvalue problem of exactly

the kind treated in §1.6 of Hinch (1991), whose approach we follow. We make the expansions

$$\boldsymbol{r} = \boldsymbol{r}_0 + b^{-1}\boldsymbol{r}_1 + \cdots, \quad \sigma = \sigma_0 + b^{-1}\sigma_1 + \cdots. \quad (C\,6)$$

The leading-order problem, $\boldsymbol{Ar}_0 = \sigma_0 \boldsymbol{r}_0$, is the circular vortex problem with eigenvalues $m \pm |m|^{1/2}$ as discussed in §1. The corresponding eigenvectors are $\boldsymbol{e}$ and the left eigenvectors are $\boldsymbol{e}^\dagger$. The $\sigma_0 = 0$ eigenvalue is multiple, so to find σ_1 we must construct from the two eigenvectors $\boldsymbol{e}_1$ and $\boldsymbol{e}_2$ the matrix $\boldsymbol{M}$ with entries

$$M_{ij} = \frac{\boldsymbol{e}_i^\dagger \cdot \boldsymbol{Be}_j}{\boldsymbol{e}_i^\dagger \cdot \boldsymbol{e}_j}, \quad (C\,7)$$

and then find its eigenvalues. The algebra is simple because the system can be truncated at $N = 1$, giving the answer $\sigma_1 = \pm 1/2$.

The approach is the same for the vortex in strain with μ replacing b^{-1} and θ replacing ξ. We need the results

$$Q(\theta) = -1 + \mu \sin n\theta + O(\mu^2), \quad G(\theta) = -1 + \mu(n+1)\sin n\theta + O(\mu^2). \quad (C\,8)$$

The matrices become

$$\boldsymbol{A} = \begin{pmatrix} i\boldsymbol{N} & -\boldsymbol{I} \\ |\boldsymbol{N}| & i\boldsymbol{N} \end{pmatrix}, \quad \boldsymbol{B} = \begin{pmatrix} \boldsymbol{S}_n\boldsymbol{N} & (n+1)\boldsymbol{S}_n\boldsymbol{N} \\ \boldsymbol{S}_n & \boldsymbol{S}_n\boldsymbol{N} \end{pmatrix}, \quad (C\,9)$$

where $\boldsymbol{S}_n$ is the matrix corresponding to $\sin n\theta$. For $n = 2$, the truncation is at $N = 1$ and the result is $\sigma_1 = \pm 1/2$. For $n = 4$, the truncation is at $N = 4$ and the result is $\sigma_1 = \pm\sqrt{2}$.

REFERENCES

ARDALAN, K., MEIRON, D. I. & PULLIN, D. I. 1995 Steady compressible vortex flows: the hollow-core vortex array. *J. Fluid Mech.* **301**, 1–17.

BAKER, G. R. 1980 Energetics of a linear array of hollow vortices of finite cross-section. *J. Fluid Mech.* **99**, 97–100.

BAKER, G. R., SAFFMAN, P. G. & SHEFFIELD, J. S. 1976 Structure of a linear array of hollow vortices of finite cross-section. *J. Fluid Mech.* **74**, 1469–1476.

BURBEA, J. 1981 On patches of uniform vorticity in a plane of irrotational flow. *Arch. Rat. Mech. Anal.* **77**, 349–358.

CROWDY, D. G. 1999 Circulation-induced shape deformations of drops and bubbles: exact two-dimensional models. *Phys. Fluids* **11**, 2836–2845.

CROWDY, D. G. & GREEN, C. C. 2011 Analytical solutions for von Kármán streets of hollow vortices. *Phys. Fluids* (in press).

DECONINCK, B. & KUTZ, J. N. 2006 Computing spectra of linear operators using the Floquet–Fourier–Hill method. *J. Comput. Phys.* **219**, 296–313.

DHANAK, M. R. 1992 Stability of a regular polygon of finite vortices. *J. Fluid Mech.* **234**, 297–316.

DRITSCHEL, D. G. 1985 The stability and energetics of corotating uniform vortices. *J. Fluid Mech.* **157**, 95–134.

HILL, D. J. 1998 Part I. Vortex dynamics in wake models. Part II. Wave generation. PhD thesis, California Institute of Technology.

HINCH, E. J. 1991 *Perturbation Methods*. Cambridge University Press.

KAMM, J. R. 1987 Shape and stability of two-dimensional uniform vorticity regions. PhD thesis, California Institute of Technology.

LEPPINGTON, F. G. 2006 The field due to a pair of line vortices in a compressible fluid. *J. Fluid Mech.* **559**, 45–55.

LUZZATTO-FEGIZ, P. & WILLIAMSON, C. H. K. 2010 Stability of conservative flows and new steady-fluid solutions from bifurcation diagrams exploiting a variational argument. *Phys. Rev. Lett.* **104**, 044504.

MACKAY, R. S. & SAFFMAN, P. G. 1986 Stability of water waves. *Proc. R. Soc. Lond.* A **406**, 115–125.

MEIRON, D. I., SAFFMAN, P. G. & SCHATZMAN, J. C. 1984 The linear two-dimensional stability of inviscid vortex streets of finite-cored vortices. *J. Fluid Mech.* **147**, 187–212.

MOORE, D. W. & PULLIN, D. I. 1987 The compressible vortex pair. *J. Fluid Mech.* **185**, 171–204.

MOORE, D. W. & SAFFMAN, P. G. 1971 Structure of a line vortex in an imposed strain. In *Aircraft Wake Turbulence and its Detection* (ed. J. A. Olsen, A Goldburg & M. Rogers), pp. 339–354. Plenum.

MOORE, D. W., SAFFMAN, P. G. & TANVEER, S. 1988 The calculation of some Batchelor flows: the Sadovskii vortex and rotational corner flow. *Phys. Fluids* **31**, 978–990.

POCKLINGTON, H. C. 1895 The configuration of a pair of equal and opposite hollow straight vortices of finite cross-section, moving steadily through fluid. *Proc. Camb. Phil. Soc.* **8**, 178–187.

SADOVSKII, V. S. 1971 Vortex regions in a potential stream with a jump of Bernoulli's constant at the boundary. *Appl. Math. Mech.* **35**, 729–735.

SAFFMAN, P. G. 1992 *Vortex Dynamics*. Cambridge University Press.

SAFFMAN, P. G. & SCHATZMAN, J. C. 1981 Properties of a vortex street of finite vortices. *SIAM J. Sci. Stat. Comput.* **2**, 285–295.

SAFFMAN, P. G. & SZETO, R. 1981 Structure of a linear array of uniform vortices. *Stud. Appl. Math.* **65**, 223–248.

SAFFMAN, P. G. & TANVEER, S. 1984 Prandtl–Batchelor flow past a flat plate with a forward facing flap. *J. Fluid Mech.* **143**, 351–365.

SEDOV, L. I. 1965 *Two-Dimensional Problems in Hydrodynamics and Aerodynamics*. Wiley.

TELIB, H. & ZANNETTI, L. 2011 Hollow wakes past arbitrarily shaped obstacles. *J. Fluid Mech.* **669**, 214–224.

THOMSON, J. J. 1883 *A Treatise on the Motion of Vortex Rings*. Macmillan.

WEGMANN, R. & CROWDY, D. 2000 Shapes of two-dimensional bubbles deformed by circulation. *Nonlinearity* **13**, 2131–2141.